On shooting methods for calculation of potential resonances

1996 J. Phys. A: Math. Gen. 29 6325

(http://iopscience.iop.org/0305-4470/29/19/017)

J. Phys. A: Math. Gen. **29** (1996) 6325–6342. Printed in the UK

On shooting methods for calculation of potential resonances

M Čížek and J Horáček

Faculty of Mathematics and Physics, Department of Theoretical Physics, Charles University Prague, V Holešovičkách 2, 180 00 Praha 8, Czech Republic

Received 26 March 1996, in final form 12 June 1996

Abstract. Two shooting methods for calculation of potential (shape) resonances are described and their efficiency tested. It is found that although both methods are based on calculation of the Siegert (i.e. exponentially increasing non-normalizable) state, the methods are stable and very accurate values of resonance energies and widths are obtainable. It is hoped that the resonance parameters obtained here can serve as test examples for various approximate methods for calculating resonance energies and widths.

1. Introduction

Resonances play an important role in many areas of physics and chemistry [1]. They manifest themselves as sharp structures in various cross sections and enhance a broad variety of processes. Let us mention just the vibrational excitation of molecules by electron impact and the dissociative attachment of electrons to molecules which are strongly influenced by the existence of short-lived negative ion states [2]. Mathematically, resonance is defined as the pole of the S-matrix lying in the lower complex half k-plane, $k_r = k_1 - ik_2$, k_1 and k_2 positive [1, 3]. Generally, there are two types of resonance [1]: Feshbach (core excited) resonances and the potential (shape) resonances. The existence of the latter is guaranteed by a special form of the interaction potential. In this paper we shall discuss only the second type of resonance.

As is well known, the resonance wavefunction is not square integrable, it diverges at large distances and its calculation is generally regarded as difficult.

To avoid the complications caused by the divergence of the resonance wavefunction at large distances the method of complex scaling in which the position vector $\boldsymbol{r}$ is rotated to the complex plane is commonly used [4–7]. For this method to be applicable the potential must satisfy certain analytic conditions which restrict its utility. The stabilization method of Hazi and Taylor, ignoring the asymptotic part of the resonance wavefunction completely, can be applied only to narrow resonances [9–19]. There exist other methods for the calculation of resonances. To mention just a few of them: the variational methods [1], the scattering methods [1, 20, 21], the Siegert method [22–27], the Riccatti–Pad method [28], the Milne method [40], the optical potential method [41], etc. The references are meant to be representative rather than exhaustive.

Here we shall discuss two methods which are different from those listed above and which to our knowledge have received little attention in the context of resonances. Both are based on the calculation of the Siegert state [22] and are of the shooting type. This means that starting from an initial guess of the resonance parameters k_1 and k_2 their value

0305-4470/96/196325+18$19.50

is iteratively improved so that the S-matrix pole is eventually found. Contrary to the aforementioned matrix methods only one resonance is calculated at a time. This is exactly what we need, since usually only one resonance dominates in a certain energy region and the distant resonances have a negligible effect on the cross section. By our methods it is possible of course to calculate all resonances in a given energy range as well as to treat overlapping resonances [29].

Computationally, the proposed two methods differ very much from each other. One method is based on the integral form of the Schrödinger equation, i.e. on the solution of the Lippmann–Schwinger equation [3], the other relies on solving the Schrödinger equation in its differential form. Both methods are based on the calculation of the Siegert state which is defined as the solution of the Schrödinger equation

$$-\psi''(r) + V(r)\psi(r) = k^2\psi(r) \tag{1}$$

(for simplicity we treat just the case $l = 0$) satisfying the following boundary conditions [22]

$$\psi_{\mathrm{S}}(k_{\mathrm{r}}, 0) = 0 \tag{2}$$

$$\frac{\psi'_{\mathrm{S}}(k_{\mathrm{r}}, R)}{\psi_{\mathrm{S}}(k_{\mathrm{r}}, R)} = \mathrm{i}k_{\mathrm{r}}. \tag{3}$$

In accordance with the usual physical conditions we assume that $V(r) = 0$ for some sufficiently large values of $r > R$. In this region the Siegert state behaves as

$$\psi_{\mathrm{S}}(k_{\mathrm{r}}, r) \sim A(k_r)\mathrm{e}^{\mathrm{i}k_{\mathrm{r}}r} \qquad \text{for } r > R \tag{4}$$

and therefore is proportional to the Jost solution $f(k_{\mathrm{r}}, r)$ [3]. As is well known the resonances arise when $k_{\mathrm{r}} = k_1 - \mathrm{i}k_2$ with k_1 and k_2 positive. For $k_1 = 0$ we have either virtual ($k_2 > 0$) or bound ($k_2 < 0$) states.

The resonance wavefunction $\psi_{\mathrm{S}}(k_{\mathrm{r}}, r)$ therefore behaves as $\psi_{\mathrm{S}}(k_{\mathrm{r}}, r) \sim A(k_{\mathrm{r}})\mathrm{e}^{\mathrm{i}k_1 r}\mathrm{e}^{k_2 r}$ at large distances where $A(k_{\mathrm{r}})$ is a function of k. Since k_2 is positive the resonance wavefunction $\psi_{\mathrm{S}}(k_{\mathrm{r}}, r)$ increases exponentially with increasing r and hence cannot be normalized in the usual way. Because of this behaviour the calculation of $\psi_{\mathrm{S}}(k_{\mathrm{r}}, r)$ is difficult, and numerical problems often arise in the course of the computation.

It is the purpose of this paper to show that an accurate and stable calculation of the resonance parameters k_1 and k_2 can be obtained by a direct calculation of $\psi_{\mathrm{S}}(k_{\mathrm{r}}, r)$ despite its asymptotic behaviour.

The paper is organized as follows. In section 2, the Schrödinger equation with the boundary condition (2), (3) is solved by the method of Gordon [45] in which the potential $V(r)$ is approximated by a piecewise linear function. This approach has been widely used for the solution of scattering problems (real k). As soon as an approximation to the potential is established, the resonance wavefunction $\psi_{\mathrm{S}}(k_{\mathrm{r}}, r)$ can be obtained in terms of the Airy functions of complex argument. The resonance parameters k_1 and k_2 are then calculated as zeros of respective Wronskians. It is found that this approach represents a very general, accurate and stable method for the calculation of resonances.

The method described in section 3, unlike the previous one, is based on the solution of the Lippmann–Schwinger equation. No approximation of the potential is made. All integrals are evaluated by means of Romberg extrapolation technique [30]. It is shown that this method is also very stable and accurate provided the resonance is narrow. If the resonance is very broad, numerical problems will occur. However, it is noteworthy to stress that only narrow resonances display themselves in cross sections and that more distant resonances (broad ones) have very small effect.

In section 4 we summarize the results and compare the efficiency of the two methods. The details of the calculation of the Airy functions are given in the appendix.

2. Differential equation approach

For the integration of the equation (1) we used the generalization of the Gordon's piecewise analytic method. This method [45] is based on dividing the range of integration into intervals $\langle x_{i-1}, x_i\rangle$, which are sufficiently small, so that the potential function $V(x)$ can be approximated by a linear function $V_{0i}(x) = c_i + d_i(x - \bar{x}_i)$ in each interval ($\bar{x}_i$ is the midpoint of interval $\langle x_{i-1}, x_i\rangle$). The best choice of $V_{0i}(x)$ (see [46]) seems to be the sum of the tangent of $V(x)$ with the weight of $\frac{1}{3}$ and the secant weighted with $\frac{2}{3}$. Excluding the trivial case $d_i = 0$, the general solution of the equation (1) with potential $V_{0i}(x)$ is a linear combination

$$\psi(x) = A\,\mathrm{Ai}(\alpha(x+\beta)) + B\,\mathrm{Bi}(\alpha(x+\beta)) \tag{5}$$

where $\mathrm{Ai}(x)$ and $\mathrm{Bi}(x)$ are the Airy functions (see the appendix), $\alpha = \sqrt[3]{d_i}$, $\beta = \frac{1}{d_i}(c_i - k^2) - \bar{x}_i$ and A, B are arbitrary constants. From this expression for $\psi(x)$ and the fact, that the Wronskian of Ai and Bi is $\frac{1}{\pi}$, it follows that

$$\psi(x_i) = \pi\left[\frac{1}{\alpha}\Delta_1\psi'(x_{i-1}) - \Delta_2\psi(x_{i-1})\right] \tag{6}$$

$$\psi'(x_i) = \pi[\Delta_3\psi'(x_{i-1}) - \alpha\Delta_4\psi(x_{i-1})] \tag{7}$$

where

$$\begin{aligned}
\Delta_1 &= \mathrm{Bi}(Z_F)\,\mathrm{Ai}(Z_I) - \mathrm{Ai}(Z_F)\,\mathrm{Bi}(Z_I)\\
\Delta_2 &= \mathrm{Bi}(Z_F)\,\mathrm{Ai}'(Z_I) - \mathrm{Ai}(Z_F)\,\mathrm{Bi}'(Z_I)\\
\Delta_3 &= \mathrm{Bi}'(Z_F)\,\mathrm{Ai}(Z_I) - \mathrm{Ai}'(Z_F)\,\mathrm{Bi}(Z_I)\\
\Delta_4 &= \mathrm{Bi}'(Z_F)\,\mathrm{Ai}'(Z_I) - \mathrm{Ai}'(Z_F)\,\mathrm{Bi}'(Z_I).
\end{aligned} \tag{8}$$

Here $Z_F = \alpha(x_i + \beta)$ and $Z_I = \alpha(x_{i-1} + \beta)$. Equations (6) and (7) are very useful expressions, which enable us to propagate ψ and ψ' from the boundary values at the origin to any point x. It is better to use (6) and (7) directly than to perform the matching of solutions (5), because Δ_i are rather small even when $\mathrm{Ai}(x)$ and $\mathrm{Bi}(x)$ are too big to be represented on a computer in common arithmetic (see the appendix).

The method is suitable for both real and complex k, but in the complex case we must be able to compute functions $\mathrm{Ai}(z)$ and $\mathrm{Bi}(z)$ for the complex values of z. In the appendix we present an algorithm for evaluating the functions $\mathrm{Ai}(z)$ and $\mathrm{Bi}(z)$ in the whole complex plane with the relative accuracy 10^{-13}. This algorithm is a generalization of the original Gordon's method to complex argument z.

In the asymptotic region outside the range R of the potential the wavefunction $\psi(k, r)$ is of the following form

$$\psi(k, r) = a_l(k)\mathrm{e}^{\mathrm{i}kr} + b_l(k)\mathrm{e}^{-\mathrm{i}kr}. \tag{9}$$

Consequently, the partial wave S-matrix, defined as the negative ratio of the coefficients $a_l(k)$ and $b_l(k)$ [31–34], is

$$S_l(k) \equiv -\frac{a_l(k)}{b_l(k)} = \frac{W(\psi(k, r), \mathrm{e}^{-\mathrm{i}kr})}{W(\psi(k, r), \mathrm{e}^{\mathrm{i}kr})} \tag{10}$$

where $W(f(r), g(r))$ denotes Wronskian of the functions $f(r)$ and $g(r)$. The poles k_r of the S-matrix are then given by the equation

$$W(k_r) = 0 \tag{11}$$

where

$$W(k) = W(\psi(k, r), e^{ikr}) \tag{12}$$

provided r lies outside the range R of the potential (then $W(k)$ is r-independent) so that (9) holds. At such values of R the Siegert eigenfunction $\psi_S(k, r)$ behaves as e^{ikr} ((4)—we assume that $\psi_S(k, r)$ is normalized so that $A(k_r) = 1$) and therefore

$$W(k) = W(\psi(k, r), \psi_S(k, r)). \tag{13}$$

The condition (11) then guarantees that the wavefunction $\psi(k, r)$ is the Siegert state. The calculation of the resonance parameters thus reduces to calculation of the Wronskian $W(k)$ and to the search for values of k_r for which $W(k_r) = 0$. The Wronskian $W(k)$ is computed from the definition

$$W(k) = W(\psi(k, r), e^{ikr}) = \psi'(k, r)e^{ikr} - ike^{ikr}\psi(k, r) \tag{14}$$

where $\psi(k, r)$ and $\psi'(k, r)$ are obtained by integration of the Schrödinger equation from the origin to the point $r = R$.

We propose to use the following method for determining the complex zeros of the function $W(z)$ [1, 35]. Let the values of the function $W(z)$ be calculated at three points z_1, z_2, z_3 (we denote them as W_1, W_2 and W_3, respectively). We construct an approximate function $W_0(z) = \frac{a_1 z + a_0}{z + b}$, so that $W_0(z_i) = W_i$ $(i = 1, 2, 3)$ (this is the Pad approximation of order [1/1]). It is easy to find the zero z_4 of the function $W_0(z)$:

$$z_4 = \frac{z_3 \frac{z_2 - z_1}{W_3} + z_2 \frac{z_1 - z_3}{W_2} + z_1 \frac{z_3 - z_2}{W_1}}{\frac{z_2 - z_1}{W_3} + \frac{z_1 - z_3}{W_2} + \frac{z_3 - z_2}{W_1}}. \tag{15}$$

Next we construct a new function $W_0(z)$, the Pad approximation to $W(z)$, so that $W_0(z_2) = W_2$, $W_0(z_3) = W_3$, $W_0(z_4) = W_4 \equiv W(z_4)$, find zero z_5 of this function and so on. Generally holds

$$z_{n+3} = \frac{z_{n+2} \frac{z_{n+1} - z_n}{W_{n+2}} + z_{n+1} \frac{z_n - z_{n+2}}{W_{n+1}} + z_n \frac{z_{n+2} - z_{n+1}}{W_n}}{\frac{z_{n+1} - z_n}{W_{n+2}} + \frac{z_n - z_{n+2}}{W_{n+1}} + \frac{z_{n+2} - z_{n+1}}{W_n}}. \tag{16}$$

The procedure is very simple and quickly converges to the exact value of the root $z = k_r$.

3. Integral equation approach

For simplicity of presentation we restrict ourselves to the case $l = 0$. The generalization to non-zero angular momentum l is straightforward. In the coordinate representation the Lippmann–Schwinger (LS) equation [3] reads

$$\psi(k, r) = \frac{\sin kr}{k} - \frac{1}{k} e^{ikr} \int_0^r \sin ky V(y) \psi(k, y)\, dy - -\frac{1}{k} \sin kr \int_r^\infty e^{iky} V(y) \psi(k, y)\, dy. \tag{17}$$

Equation (17) is of the Fredholm type. It is worthwhile considering instead of this equation another integral equation defining the so-called regular solution [3]

$$\phi(k, r) = \frac{\sin kr}{k} - \frac{1}{k} \int_0^r (e^{ikr} \sin ky - e^{iky} \sin kr) V(y) \phi(k, y)\, dy \tag{18}$$

which is of the Voltera type and can be solved very easily [30]. Once the solution $\phi(k,r)$ is known the physical solution $\psi(k,r)$ can be expressed as

$$\psi(k,r) = \frac{\phi(k,r)}{1+\int_0^\infty \mathrm{e}^{\mathrm{i}kr}V(r)\phi(k,r)\,\mathrm{d}r}. \tag{19}$$

Similarly we can express the T-matrix in terms of $\phi(k,r)$ as

$$T(k) = \frac{\int_0^\infty \sin kr\,V(r)\phi(k,r)\,\mathrm{d}r}{1+\int_0^\infty \mathrm{e}^{\mathrm{i}kr}V(r)\phi(k,r)\,\mathrm{d}r}. \tag{20}$$

The T-matrix has a pole when the denominator (the Jost function) in (20) vanishes:

$$0 = 1+\int_0^\infty \mathrm{e}^{\mathrm{i}kr}V(r)\phi(k,r)\,\mathrm{d}r. \tag{21}$$

To calculate the resonance pole we vary the (complex) momentum k until the condition

$$F(k_\mathrm{r}) = -1 \tag{22}$$

where

$$F(k,r) = \int_0^r \mathrm{e}^{\mathrm{i}kr}V(r)\phi(k,r)\,\mathrm{d}r \qquad \text{and} \qquad F(k) = F(k, r\to\infty) \tag{23}$$

is satisfied. The calculation is performed on a set of grids with an increasing number of grid points, and, with the use of Romberg extrapolation [30] very accurate values of $F(k)$ can be obtained. One word of caution is necessary here. As we know, the wavefunction $\phi(k = k_1 - \mathrm{i}k_2, r)$ behaves as

$$\phi(k,r) \sim A(k)\mathrm{e}^{\mathrm{i}k_1 r}\mathrm{e}^{k_2 r} \tag{24}$$

at large distances. The integrand in (23) attains the form ($r\to\infty$)

$$\sim A(k)\mathrm{e}^{2\mathrm{i}k_1 r}\mathrm{e}^{2k_2 r}V(r). \tag{25}$$

Let us assume for a while that the potential is exponentially decreasing

$$V(r) \sim V_0\mathrm{e}^{-\alpha r}. \tag{26}$$

Then for the integral (23) to exist (the same holds for analogous integrals in (18)) we must demand that

$$k_2 < \frac{\alpha}{2}. \tag{27}$$

This means that only resonances with small values of k_2 (narrow resonances) can be determined in this way. For details we refer to [3].

4. Results

4.1. Analytic potentials

As a first test we apply both methods to a simple smooth analytic potential

$$V(r) = \lambda r^2\mathrm{e}^{-r} \tag{28}$$

which serves a standard test and which has been studied by various methods in many papers (see for example [15, 23, 24, 26, 28, 36–40]). Table 1 shows the calculated resonance energies and widths for a series of values of the parameter λ. Both methods yielded identical values and the results are probably correct to all figures printed in this table. The cut-off radius R is 40 for $\lambda < 8$ and $R = 25$ for the rest of the values.

Table 1. Resonance energies and widths for the potential (28).

λ	E_r	$\Gamma/2$	λ	E_r	$\Gamma/2$
3	0.973 823 63	−2.154 0507 − 1	15	3.426 390 31	−1.277 4480 − 2
4	1.234 208 72	−1.872 2802 − 1	16	3.587 033 69	−9.186 4904 − 3
5	1.477 948 26	−1.591 1786 − 1	17	3.742 927 77	−6.543 5906 − 3
6	1.708 912 74	−1.327 9218 − 1	18	3.894 398 85	−4.624 2840 − 3
7	1.929 400 36	−1.089 9823 − 1	19	4.041 763 72	−3.247 1588 − 3
8	2.140 879 36	−8.803 9256 − 2	20	4.185 323 29	−2.268 8374 − 3
9	2.344 336 68	−6.998 0354 − 2	21	4.325 357 91	−1.579 3618 − 3
10	2.540 466 03	−5.474 1130 − 2	22	4.462 124 84	−1.096 4761 − 3
11	2.729 781 15	−4.214 3870 − 2	23	4.595 857 56	−7.598 7596 − 4
12	2.912 689 66	−3.194 4009 − 2	24	4.726 766 46	−5.260 5566 − 4
13	3.089 542 94	−2.385 4326 − 2	25	4.855 040 35	−3.640 2136 − 4
14	3.260 668 79	−1.756 7059 − 2	26	4.980 848 50	−2.519 0637 − 4

Table 2. Convergence of the Romberg extrapolation for the potential (28) (integral equation method); N is the number of meshpoints and λ is the potential strength.

	λ = 4		λ = 15		λ = 24	
	E_r	$\Gamma/2$	E_r	$\Gamma/2$	E_r	$\Gamma/2$
N	1.233 214 410	0.188 041 3989	3.420 855 746	1.365 490 260 − 2	4.719 388 561	6.273 899 787 − 4
$2N$	1.234 208 121	0.187 230 6240	3.426 343 540	1.284 183 606 − 2	4.726 594 816	6.666 582 961 − 4
$4N$	1.234 208 267	0.187 228 1932	3.426 390 315	1.277 462 929 − 2	4.726 766 178	5.268 962 929 − 4
$8N$	1.234 208 272	0.187 228 1874	3.426 390 313	1.277 448 057 − 2	4.726 766 464	5.260 563 327 − 4
$16N$	1.234 208 269	0.187 228 1907	3.426 390 313	1.277 448 017 − 2	4.726 766 459	5.260 556 580 − 4

As expected, the resonances become narrower with increasing λ. In table 2 we show the results obtained with the integral equation method, in order to display the stability of the method by changing the number of grid points. As usual in the Romberg extrapolation technique one solves the problem at a series of grids using $N, 2N, 4N, 8N, \ldots$ grid points and then extrapolates the results. In all the rest of the calculations we used $R = 25$.

N is the starting number of the grid points, here $N = 100$. We see that very accurate results can be obtained in this way keeping the number of mesh points moderately low (no optimization of the grid was performed). The results obtained with the differential equation method are collected in table 3. Here M denotes the number of segments into which the integration range $\langle 0, 25\rangle$ was partitioned. No extrapolation was performed. We have used a non-equidistant grid defined as

$$x_i = R\frac{\mathrm{e}^{\mathrm{i}Q/M} - 1}{\mathrm{e}^{Q} - 1} \qquad \text{with } Q = 3. \tag{29}$$

The resulting resonance parameters are again stable with increasing number of meshpoints and we see that very accurate values are obtainable.

In figures 1–3 we plot the calculated wavefunctions for three values of the potential strengths λ. Figure 1 describes a very narrow resonance ($E = 4.727 - \mathrm{i}0.000\,5261$) which was obtained with $\lambda = 24$. The full curve depicts the real part of the wavefunction of the Siegert state, the potential is plotted (arbitrary units) by the short broken curve and the function $F(k, r)$, (23), by long the long broken curve. As expected the wavefunction is strongly localized. In figure 2 a broader resonance ($E = 3.426 - \mathrm{i}0.012\,77$) obtained

Table 3. Convergence of the differential equation method for the potential (28); M is the number of meshpoints and λ is the potential strength.

	$\lambda = 4$		$\lambda = 15$		$\lambda = 24$	
M	E_r	$\Gamma/2$	E_r	$\Gamma/2$	E_r	$\Gamma/2$
10	1.233 322 830	0.162 945 4084	3.425 121 791	1.329 627 062 − 2	4.727 539 144	5.260 281 379 − 4
20	1.231 258 313	0.186 530 3053	3.426 524 972	1.283 143 745 − 2	4.726 866 514	5.232 207 315 − 4
50	1.234 205 623	0.187 229 0096	3.426 389 168	1.277 487 138 − 2	4.726 768 897	5.260 663 579 − 4
100	1.234 208 104	0.187 228 2365	3.426 390 240	1.277 450 272 − 2	4.726 766 610	5.260 571 914 − 4
200	1.234 208 258	0.187 228 1914	3.426 390 305	1.277 448 185 − 2	4.726 766 466	5.260 557 598 − 4
400	1.234 208 267	0.187 228 1886	3.426 390 310	1.277 448 055 − 2	4.726 766 457	5.260 556 703 − 4

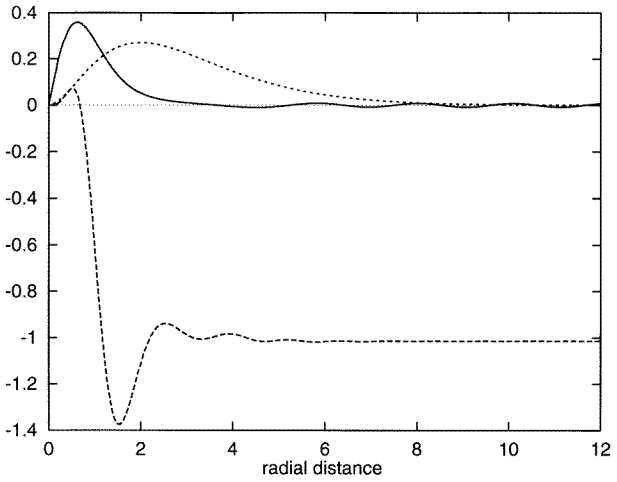

Figure 1. Plot of the wavefunction corresponding to the Siegert state for the potential, (28), with λ=24. Full curve, the real part of the wavefunction, short broken curve, the potential (arbitrary units), long broken curve, the function $F(k, r)$ defined in (23).

with $\lambda = 15$ is shown and finally in figure 3 the wavefunction of a very broad resonance ($E = 1.477 - i0.159$) generated with $\lambda = 4$ is plotted. In the last case the amplitude of the Siegert state increases rapidly with the radial distance.

4.2. Non-analytic potentials

As the second test we apply both methods to a non-analytic potential

$$V(r) = 30\frac{r-b}{\sqrt{|r-b|}}e^{-r}. \tag{30}$$

This potential is smooth and finite everywhere but at the point $r = b$ its derivative diverges, simulating in this way a hard-core potential (see figure 4). The results of the calculation of the resonance parameters obtained both with the integral and differential equation approach are shown in tables 4 and 5 for two values of parameter b. No attempt was made to choose the point $x = b$ as a grid point.

It is clear that the convergence is much worse than in the previous case because of the non-analyticity of the potential. It is worthwhile mentioning however, that the complex scaling methods widely used in atomic physics cannot be applied in this case.

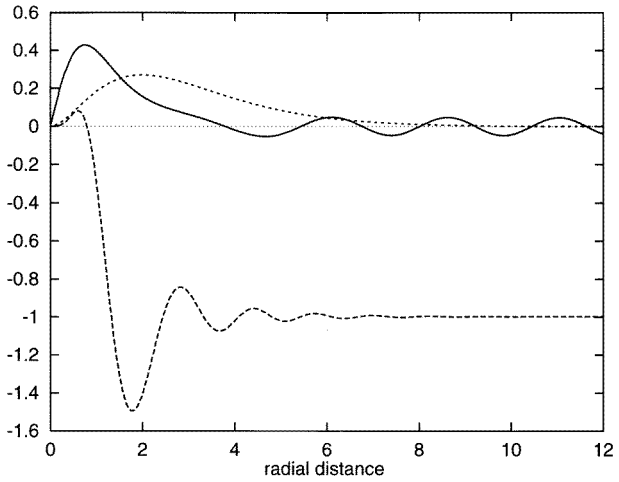

Figure 2. The same as in figure 1 but for a broader resonance generated with $\lambda = 15$.

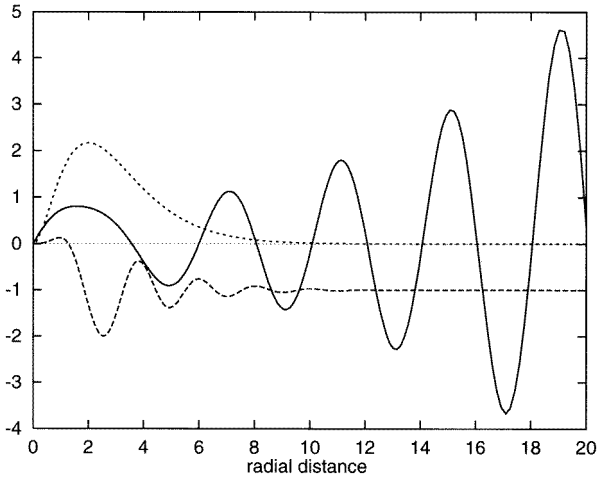

Figure 3. The same as in figure 1 but for a broad resonance obtained with $\lambda = 4$.

Table 4. Convergence for the non-analytic potential (30) (integral equation approach); N is the number of meshpoints.

	$b = 0.4$		$b = 0.65$	
$N = 100$	E_r	$\Gamma/2$	E_r	$\Gamma/2$
N	4.016 684 270	0.242 935 7339	0.466 468 5418	2.987 535 648 − 5
$2N$	4.011 636 114	0.237 693 6854	0.460 552 8461	2.556 730 078 − 5
$4N$	4.009 152 168	0.236 873 2119	0.469 972 9324	3.114 596 597 − 5
$8N$	4.008 257 293	0.236 572 3614	0.468 599 8089	2.973 623 393 − 5
$16N$	4.007 978 214	0.236 478 1074	0.468 153 5929	2.968 887 162 − 5
$32N$	4.008 155 858	0.236 538 4153	0.468 121 7736	2.968 612 743 − 5

4.3. Singular potentials

As a prototype of a singular potential we choose the combination of two Yukawa-type potentials

$$V(r) = -100\frac{e^{-4r}}{r} + \lambda\frac{e^{-r}}{r} \tag{31}$$

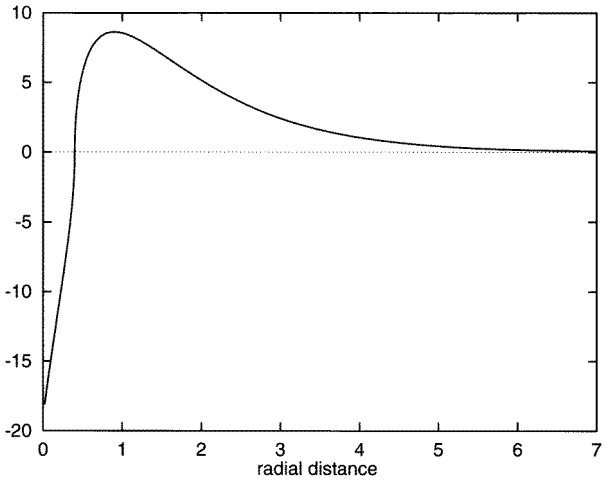

Figure 4. Potential function: $V(r) = 30\frac{r-b}{\sqrt{|r-b|}}\mathrm{e}^{-r}$.

Table 5. Convergence for non-analytic potential (30) (differential equation approach); M is the number of meshpoints.

	$b = 0.4$		$b = 0.65$	
M	E_r	$\Gamma/2$	E_r	$\Gamma/2$
100	4.009 628 532	0.237 025 4798	0.480 023 805	3.200 759 620 − 5
200	4.006 155 876	0.235 859 0517	0.468 132 011	2.968 711 859 − 5
400	4.006 742 046	0.236 060 3477	0.467 233 679	2.951 917 410 − 5
800	4.008 039 402	0.236 498 8148	0.468 568 725	2.977 054 869 − 5
1600	4.008 204 154	0.236 554 7512	0.468 119 594	2.968 577 128 − 5
3200	4.008 259 417	0.236 573 5115	0.468 071 669	2.967 674 747 − 5

with variable λ. This potential is singular at the origin and has a rich resonance structure. All Siegert states are bound states for $\lambda = 0$; at increasing λ the repulsive barrier is subsequently built and resonances appear. As λ approaches the value $\lambda \sim 15$ a pair of S-matrix poles, one bound-state pole and one virtual-state pole, appear very close to the threshold. These poles move in opposite directions along the imaginary axis at increasing λ and coalesce at some value $\lambda_\mathrm{c} \doteq 15.030\,34$ ($R = 30$). At increasing λ, $\lambda > \lambda_\mathrm{c}$, the poles again separate and their trajectories form two symmetric branches in the lower complex half plane. This behaviour allows us to expose our approach to the more difficult case of two very close poles of the S-matrix (so far we have been treating only isolated poles). We performed a series of calculations of the S-matrix poles with the integral equation approach for a range of values of λ from the region of a weakly bound state to the appearance of a narrow resonance including values of λ for which both poles merge. It is found that again very accurate and stable results are obtained with our approach even in the case of merging poles and singular potentials. The results are collected in the table 6 which shows the locations of the two poles versus the coupling parameter λ.

Table 6. S-matrix poles for the singular potential (31).

λ	$\mathrm{Re}\,k_\mathrm{r}$	$\mathrm{Im}\,k_\mathrm{r}$	$\mathrm{Re}\,k_\mathrm{r}$	$\mathrm{Im}\,k_\mathrm{r}$
15.00	0.0	0.2118	0.0	−0.2251
15.01	0.0	0.1718	0.0	−0.1859
15.02	0.0	0.1201	0.0	−0.1349
15.03	0.0	0.0155	0.0	−0.0312
15.035	0.0854	−0.0080	−0.0854	−0.0080
15.04	0.1231	−0.0082	−0.1231	−0.0082
15.05	0.1755	−0.0086	−0.1755	−0.0086
15.10	0.3301	−0.0106	−0.3301	−0.0106
16.00	1.2059	−0.0568	−1.2059	−0.0568

4.4. Location of resonances

A widely used method for calculating the resonance parameters is based on the parametrization of the cross section (phase shift) in the vicinity of a resonance by the Breit–Wigner formula [1] or more generally by an analytic representation of the S-matrix [20]. As is well known, the phase shift increases rapidly in the resonance region. If the resonance is narrow the phase shift increases by π on a very narrow energy range. Since the phase shift is determined only modulo π it is necessary to repeat the calculation with very small energy steps otherwise the resonance may easily be overlooked. This results in a huge increase in volume of the computation and sometimes even special procedures for the location of very narrow resonances must be used [21].

However, if we look at the function $F(k)$, defined by (23), we find (the same also holds for the Wronskian $W(k)$) that $F(k)$ is a very smooth function of k and the location of the resonance position is easy even for very narrow resonances. This is clearly demonstrated in figure 5 which shows the real part of $F(k)+1$ and the imaginary part of $F(k)$ plotted

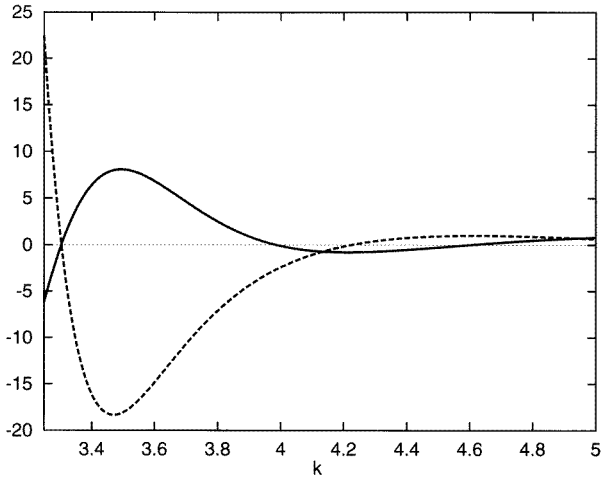

Figure 5. The real (full curve) and imaginary (broken curve) parts of the Jost function $1+F(k)$, (23), for the potential (28) with $\lambda = 30$ plotted for real k. The two lines cross around $k = 3.3$ in correspondence with the presence of a very narrow resonance at $k = 3.305 - i0.000\,0176$. The broader resonances above $k = 4.2$ are also seen.

for a range of real k calculated with the potential 28 with $\lambda = 30$. The full curve shows the $\mathrm{Re}(F(k) + 1)$, the broken curve that of $\mathrm{Im}(F(k))$. Both lines cross near $k = 3.30$ (this corresponds to the resonance at $k = 3.305 - i0.000\,0176$). The second resonance (at $k = 4.179 - i0.128$) is also seen. Now, however, the two curves do not cross at one real point and the distance between the roots is a measure of the resonance width Γ. For comparison we plot the cross section and the phase shift in figure 6. It follows from figure 5 that even if we are far away from the resonance the zero of $F(k)$ is easily discernible and with a very few sample points the position of the resonance can be located even for very narrow resonances. Hence, a very sparse energy grid may be used to locate the resonance reducing considerably the amount of the numerical work.

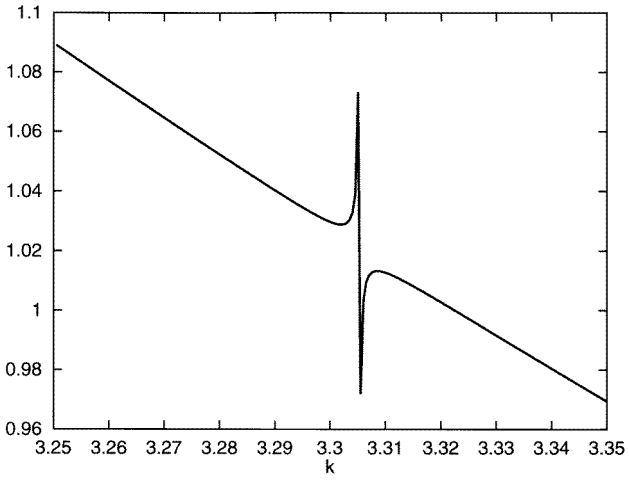

Figure 6. The cross section in the region of the narrow resonance discussed in figure 5. Note difference in the scales.

4.5. Calculation of zeros of the function $W(k)$

As is well known, each potential identically equal to zero for $r > R$, where R is a finite non-zero value, provides an infinite number of resonances, so-called cut-off resonances. These resonances can easily be separated from the true ones by their large sensitivity to changes of the parameter R. Therefore, the number of resonance poles in a given region may be large.

As described above, the resonance poles, i.e. zeros of $W(k)$ are localized iteratively by means of the Pad [1/1] approximation. To start this procedure three points z_1, z_2 and z_3 in the vicinity of the resonance pole must be provided. Usually we choose the points on a circle of a small radius. If the resonance pole is located inside or in the proximity of the circle the process of finding the root of the Wronskian is very fast, and just a few iterations lead to a very accurate determination of the root. However, if the initial guess was wrong, i.e. at a considerable distance from the pole, the number of iterations increases and not always the pole closest to the starting value is found. Sometimes even a very distant pole may be found in this way. To see how the choice of the starting point influences the calculation we applied the method to some simple analytic functions. As the first test we take the function $g(z) = z^4 - 1$, which has four zeros $z = \pm 1$ and $z = \pm \mathrm{i}$. Let z_0 denote the centre of a circle on which z_1, z_2 and z_3 lie and let us investigate four domains of z_0

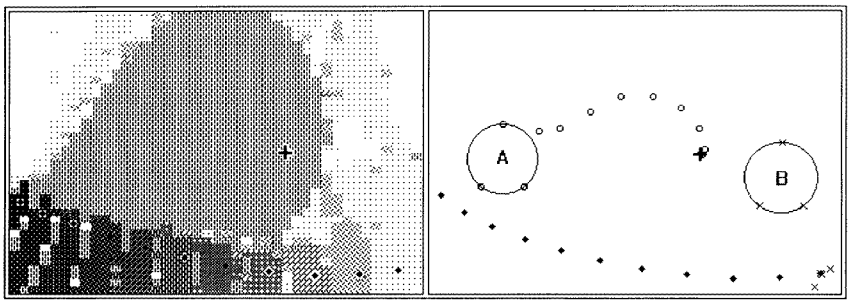

Figure 7. Poles of the Wronskian for potential $15r^2e^{-r}$ with the cut-off $R = 15$. The true pole is indicated by a cross, and cut-off poles with dots. Domains leading to the different poles are plotted in the left figure. Two traces of the Pad method for two different initial guesses A and B are shown on the right.

in the complex plane, which lead to those four zeros. It turns out that boundaries among them are approximately the rays $\arg(z_0) = (2n + 1)\frac{\pi}{4}$ with n integer, but the behaviour of the method is highly unstable near the rays and it is very difficult to say which zero will be reached if z_0 is taken from this region.

The picture is much more complicated for realistic calculations, however. This is shown in figure 7. Roots of the Wronskian $W(k)$ and respective domains are plotted in figure 7(a) for the potential $V(x) = 15x^2e^{-x}$. In figure 7(b) we follow the trace of the Pad [1/1] approximant. The trace started from the circle A (denoted by the small circles) converges to the true resonance, but the trace B (crosses) leads to the cut-off resonance.

Other methods for determining complex zeros (for example the Newton–Raphson method) show analogous complicated behaviour [42].

5. Conclusions

We have implemented and tested two numerical methods for calculating the S-matrix poles for local short-range potentials. The S-matrix poles are defined here as the Siegert states [22].

The first method is based on the idea of approximating the potential by a piecewise linear function. To implement this idea an efficient method of calculating Airy functions for complex arguments is necessary. By generalizing Gordon's method [45] we developed a very fast and accurate method of calculating Airy functions (details are described in the appendix). By using this algorithm the resonance poles can be calculated accurately as the zeros of the Wronskian $W(k)$, (11). By treating potentials with increasing complexity it was shown in examples that very accurate and stable results are obtained (see tables 1–5) with a moderate number of partitions of integration range R provided the resonance is not very broad or the integration range is not very long. In this way we confirm the findings of Meyer and Walter [26] who state that all methods based on the Schrödinger equation lose their stability for $\mathrm{Re}(\mathrm{i}kr) > 17$ (using 16-digit arithmetic). In this paper we made no attempt to use the long-range corrections of Meyer and Walter [26].

The second approach tested here is based on the solution of the integral equation (18). The integration range is discretized and all the calculations are performed on a grid. No approximation of the potential is performed. The calculations are repeated on various grids and by means of the Romberg extrapolation very precise results are obtained. It appears that

Table 7. Convergence of the integral equation approach for a broad resonance in the potential $V(r) = 15r^2e^{-r}$; R denotes the range of integration.

R	Re k	Im k
10	3.125 2062	−0.231 1916
20	3.132 4457	−0.304 5132
40	3.132 1414	−0.353 0260
60	3.130 0853	−0.357 1228
80	3.130 0427	−0.357 1442
100	3.130 0425	−0.357 1443
200	3.130 0425	−0.357 1443
300	3.130 0425	−0.357 1443

for resonances with small Re(k)((Re(k) < 10) the number of meshpoints needed for the required accuracy is usually low (for example 100, 200 and 400 not optimized points yields six-figure accuracy for potential of (28)). For resonances with higher Re(k) the differential equation approach may be more efficient. However, the integral equation approach has a definite advantage over the differential equation approach: it is much more stable and the condition Re(ikR) > 17 may be relaxed. To see this we present here the calculation of the second non-cut-off pole generated by the potential $V(r) = 15r^2e^{-r}$ in table 7.

Our results are stable even for $R > 300$ (i.e. Re(ikR) > 100) and compare well with values ($k = 3.130 - i0.357$) quoted by Meyer and Walter [26]. In all the cases studied above it was assumed that the potential was local. It is known, however, that many physically interesting potentials possess significant non-local parts [3]. To treat such potentials the method discussed above must be generalized.

Appendix

A.1. Airy functions

The Airy functions Ai(z) and Bi(z) can be defined as sums of the following power series (see [47])

$$\mathrm{Ai}(z) = c_1 f(z) - c_2 g(z) \tag{32}$$

$$\mathrm{Bi}(z) = \sqrt{3}[c_1 f(z) + c_2 g(z)] \tag{33}$$

where

$$f(z) = 1 + \frac{1}{3!}z^3 + \frac{1.4}{6!}z^6 + \frac{1.4.7}{9!}z^9 + \cdots \tag{34}$$

$$g(z) = z + \frac{2}{4!}z^4 + \frac{2.5}{7!}z^7 + \frac{2.5.8}{10!}z^{10} + \cdots \tag{35}$$

and

$$c_1 = \frac{1}{2\pi}\Gamma\left(\frac{1}{3}\right)3^{-\frac{1}{6}} \qquad c_2 = \frac{1}{2\pi}\Gamma\left(\frac{2}{3}\right)3^{\frac{1}{6}}. \tag{36}$$

The convergence radius of these series is infinite. However, the functions Ai(z) and Bi(z) cannot be evaluated by means of (32)–(36) in the whole complex plane. For large $|z|$, these series are very slowly convergent and cancellation of terms occurs in the regions where values of the functions are small.

A.2. Evaluation of $Ai(x)$ and $Bi(x)$ for real x

Gordon [45] has derived formulae (43)–(46) (see below), which lead to a very efficient and precise method for evaluating Airy functions and expressions containing them for real values of x. Let us start with integral expressions [45] for $\mathrm{Ai}(x)$ and $\mathrm{Bi}(x)$

$$\mathrm{Ai}(x) = \frac{1}{2\sqrt{\pi}} x^{-\frac{1}{4}} \mathrm{e}^{-\xi} \int_0^\infty \frac{\rho(t)\,\mathrm{d}t}{1+(t/\xi)} \tag{37}$$

$$\mathrm{Bi}(x) = \frac{1}{\sqrt{\pi}} x^{-\frac{1}{4}} \mathrm{e}^{+\xi} \int_0^\infty \frac{\rho(t)\,\mathrm{d}t}{1-(t/\xi)} \tag{38}$$

$$\mathrm{Ai}(-x) = \frac{1}{\sqrt{\pi}} x^{-\frac{1}{4}} \int_0^\infty \frac{\cos(\xi-\frac{\pi}{4}) + (t/\xi)\sin(\xi-\frac{\pi}{4})}{1+(t/\xi)^2} \rho(t)\,\mathrm{d}t \tag{39}$$

$$\mathrm{Bi}(-x) = \frac{1}{\sqrt{\pi}} x^{-\frac{1}{4}} \int_0^\infty \frac{(t/\xi)\cos(\xi-\frac{\pi}{4}) - \sin(\xi-\frac{\pi}{4})}{1+(t/\xi)^2} \rho(t)\,\mathrm{d}t \tag{40}$$

where x is real positive,

$$\xi = \tfrac{2}{3}x^{\frac{3}{2}} \qquad \text{and} \qquad \rho(t) = \pi^{-\frac{1}{2}} 2^{-\frac{1}{6}} 3^{\frac{1}{6}} t^{-\frac{5}{6}} \mathrm{e}^{-t}\, \mathrm{Ai}((\tfrac{3}{2}t)^{\frac{2}{3}}). \tag{41}$$

Using the fact that moments μ_k of the weight function $\rho(x)$ are known [43]

$$\mu_k \equiv \int_0^\infty x^k \rho(x)\,\mathrm{d}x = \frac{\Gamma(3k+\frac{1}{2})}{54^k k!\Gamma(k+\frac{1}{2})} \tag{42}$$

we can use the method of the generalized Gaussian quadrature [44] to evaluate integrals in (37) and (38), which leads to

$$\mathrm{Ai}(x) \doteq \frac{1}{2\sqrt{\pi}} x^{-\frac{1}{4}} \mathrm{e}^{-\xi} \sum_{i=1}^{n} \frac{w_i}{1+\frac{x_i}{\xi}} \tag{43}$$

$$\mathrm{Bi}(x) \doteq \frac{1}{\sqrt{\pi}} x^{-\frac{1}{4}} \mathrm{e}^{+\xi} \sum_{i=1}^{n} \frac{w_i}{1-\frac{x_i}{\xi}} \tag{44}$$

$$\mathrm{Ai}(-x) \doteq \frac{1}{\sqrt{\pi}} x^{-\frac{1}{4}} \sum_{i=1}^{n} w_i \frac{\cos(\xi-\frac{\pi}{4}) + \frac{x_i}{\xi}\sin(\xi-\frac{\pi}{4})}{1+(\frac{x_i}{\xi})^2} \tag{45}$$

$$\mathrm{Bi}(-x) \doteq \frac{1}{\sqrt{\pi}} x^{-\frac{1}{4}} \sum_{i=1}^{n} w_i \frac{\frac{x_i}{\xi}\cos(\xi-\frac{\pi}{4}) - \sin(\xi-\frac{\pi}{4})}{1+(\frac{x_i}{\xi})^2}. \tag{46}$$

Values of the nodes x_i and weights w_i for $n = 10$ can be taken from [45] and for $n = 20$ (our result) are given in the table 8:

This allows us to calculate $\mathrm{Ai}(x)$ and $\mathrm{Bi}(x)$ on the whole real axis using (43)–(46), except close to the origin, where the error of these expressions increases and the series (32)–(36) must be used. Corresponding intervals (according to Gordon [45]) for relative precision 10^{-14} (using 16-digits arithmetic) are given in table 9. In fact the relative error of $ai(x)$ is slightly higher ($\sim 10^{-12}$) near $x = 3.7$ due to cancellation of terms in the power series. So we recommend using (43) with $n = 20$ for $x \in \langle 2.14, 4.2\rangle$ if a really high precision is required.

For solving the Schrödinger equation only the quantities Δ_i are directly required, not the values of the Airy functions, see (6) and (7). It is not very convenient to compute Airy functions first and then to use (8), because values of $\mathrm{Ai}(x)$ are very small and values of $\mathrm{Bi}(x)$ very big for large positive x and both functions are highly oscillatory for large negative x. It is much better to substitute expressions (43)–(46) into (8) instead and collect exponential or oscillatory terms, which nearly cancel out.

Table 8. Weights and nodes for evaluation of the Airy functions (equations (43)–(46)).

	i	w_i	x_i
$n = 20$	1	$7.367\,629\,917\,890\,1838 \times 10^{-1}$	$4.138\,104\,596\,959\,3848 \times 10^{-3}$
	2	$1.637\,323\,588\,744\,4356 \times 10^{-1}$	$1.014\,067\,838\,903\,4257 \times 10^{-1}$
	3	$6.570\,004\,475\,518\,6294 \times 10^{-2}$	$3.205\,073\,781\,659\,7486 \times 10^{-1}$
	4	$2.411\,813\,173\,090\,3074 \times 10^{-2}$	$6.638\,935\,637\,889\,6527 \times 10^{-1}$
	5	$7.419\,250\,357\,169\,8453 \times 10^{-3}$	$1.134\,300\,624\,683\,1197$
	6	$1.843\,764\,790\,888\,4445 \times 10^{-3}$	$1.735\,088\,919\,269\,7992$
	7	$3.616\,318\,396\,044\,2296 \times 10^{-4}$	$2.470\,526\,438\,097\,2342$
	8	$5.491\,243\,708\,738\,4324 \times 10^{-5}$	$3.346\,026\,679\,221\,7012$
	9	$6.334\,261\,117\,425\,5159 \times 10^{-6}$	$4.368\,419\,128\,0619\,897$
	10	$5.437\,206\,860\,231\,9701 \times 10^{-7}$	$5.546\,303\,499\,989\,5683$
	11	$3.390\,641\,438\,271\,3043 \times 10^{-8}$	$6.890\,543\,640\,208\,1020$
	12	$1.491\,946\,218\,236\,8753 \times 10^{-9}$	$8.414\,983\,529\,145\,1491$
	13	$4.465\,712\,145\,839\,1191 \times 10^{-11}$	$10.137\,524\,095\,983\,333$
	14	$8.671\,110\,960\,163\,8167 \times 10^{-13}$	$12.081\,813\,157\,473\,574$
	15	$1.024\,660\,028\,979\,5361 \times 10^{-14}$	$14.280\,042\,673\,374\,010$
	16	$6.736\,064\,233\,908\,1152 \times 10^{-17}$	$16.777\,910\,032\,636\,809$
	17	$2.153\,990\,102\,811\,0840 \times 10^{-19}$	$19.644\,275\,859\,114\,523$
	18	$2.690\,146\,409\,301\,3610 \times 10^{-22}$	$22.992\,627\,728\,392\,780$
	19	$8.668\,109\,035\,110\,7345 \times 10^{-26}$	$27.039\,719\,919\,610\,232$
	20	$2.542\,001\,893\,424\,9125 \times 10^{-30}$	$32.341\,049\,358\,350\,355$

Table 9. Ranges for evaluation of $\mathrm{Ai}(x)$ and $\mathrm{Bi}(x)$ for real x.

	Ai	Bi
$x \in (\infty, -5\rangle$	(45) for $n = 10$	(46) for $n = 10$
$x \in \langle -5, 3.7\rangle$	Power series	Power series
$x \in \langle 3.7, 8\rangle$	(43) for $n = 10$	Power series
$x \in \langle 8, \infty)$	(43) for $n = 4$	(44) for $n = 4$

A.3. Analytic continuation of the Gordon's method

We shall see that formulae (43) and (44) cannot be used directly with real positive x replaced by complex z. The formulae were obtained from (37)–(40) by means of Gaussian quadrature so we will examine the analytic continuation of (37)–(40).

Let us start with expression (37). The right-hand side of this equation is analytical in the domain $D = \{z, |\arg(z)| < \frac{2}{3}\pi\}$. The integral path must be deformed to circumvent the pole $t = \frac{2}{3}z^{\frac{3}{2}}$, when z is from the rest of the complex plane. The resulting contour integral can be written as integral over the positive real axis plus the respective residuum. Thus for $\pm\arg(z) > \frac{2}{3}\pi$:

$$\mathrm{Ai}(z) = \frac{1}{2\sqrt{\pi}} z^{-\frac{1}{4}} \mathrm{e}^{-\xi} \int_0^\infty \frac{\rho(t)\,\mathrm{d}t}{1 + (t/\xi)} + \delta_1^{(\pm)}(z) \tag{47}$$

where

$$\delta_1^{(\pm)}(z) = \mp \mathrm{i}\pi^{\frac{1}{2}} z^{-\frac{1}{4}} \mathrm{e}^{-\xi}\, \mathrm{Rez}_{t=-\xi} \frac{\rho(t)}{1 + (t/\xi)} \tag{48}$$

and

$$\xi = \tfrac{2}{3}z^{\frac{3}{2}} = \tfrac{2}{3}|z|^{\frac{3}{2}} \mathrm{e}^{\frac{3\mathrm{i}}{2}\arg(z)}. \tag{49}$$

Function $\delta_1^{\pm}$ for $|\arg(z)| > \frac{2}{3}\pi$ can be evaluated explicitly in terms of $\mathrm{Ai}(\eta)$, where η is in the domain D so that (37) can be used. In this way we find that (47) coincides with (39).

Treating (39) and (40) in the same way, we discover that these expressions are valid in the domain $|\arg(z)| < \frac{\pi}{3}$ and must be modified for $\pm\arg(z) > \frac{\pi}{3}$ adding the factors $\delta_3^{\pm}(z)$ and $\delta_4^{\pm}(z)$ respectively to the right-hand sides. The situation is slightly different for the equation (38) because the right-hand side is a principal value integral. However, it can be shown that (for $\pm\arg(z) > 0$)

$$\mathrm{Bi}(z) = \frac{1}{\sqrt{\pi}} z^{-\frac{1}{4}} \mathrm{e}^{+\xi} \int_0^{\infty} \frac{\rho(t)\,\mathrm{d}t}{1-(t/\xi)} + \delta_2^{(\pm)}(z) \tag{50}$$

with

$$\delta_2^{(\pm)}(z) = \mp \mathrm{i}\pi^{\frac{1}{2}} z^{-\frac{1}{4}} \mathrm{e}^{+\xi}\, \mathrm{Rez}_{t=\xi} \frac{\rho(t)}{1-(t/\xi)}. \tag{51}$$

Similarly as for $\mathrm{Ai}(z)$ it can be shown that (50) leads to (40) on the negative real axis.

One way of evaluating $\mathrm{Ai}(z)$ in the complex plane is a direct use of (43) in the domain D and of (45) elsewhere. It seems at first sight, that the Gaussian quadrature of integral (37) or (39) will not work near the rays $\arg(z) = \pm\frac{2}{3}\pi$, because of the proximity of the poles to the integration path. Fortunately $\delta_1^{\pm}$ is exponentially damped in this region and the error of the Gaussian quadrature due to proximity of the pole is proportional to $\delta_1^{\pm}$. It is the same situation as in the formula (38) on the real axis and in (39) and (40) near the rays $\arg(z) = \pm\frac{\pi}{3}$ and so $\mathrm{Bi}(z)$ could be treated similarly. But this way of evaluating the Airy functions is not the best one, which is clearly seen from the fact that formula (44) is of use for $x > 8$ only (table 9). We prefer to evaluate functions $\mathrm{Ai}(z)$ and $\mathrm{Bi}(z)$ in a different manner.

The following relations hold for the Airy functions of the rotated argument [47]:

$$\mathrm{Ai}(z\mathrm{e}^{\pm\frac{2}{3}\pi\mathrm{i}}) = \tfrac{1}{2}[\mathrm{Ai}(z) \mp \mathrm{i}\,\mathrm{Bi}(z)] \tag{52}$$

$$\mathrm{Bi}(z\mathrm{e}^{\pm\frac{2}{3}\pi\mathrm{i}}) = \tfrac{1}{2}[\mathrm{Bi}(z) \mp 3\mathrm{i}\,\mathrm{Ai}(z)]. \tag{53}$$

This can also be seen directly from the definition (32)–(35). From these relations we can evaluate $\mathrm{Ai}(z)$ and $\mathrm{Bi}(z)$ in the whole complex plane knowing $\mathrm{Ai}(z)$ only in $\{z, |\arg(z)| \leqslant \frac{\pi}{3}\}$ and $\mathrm{Bi}(z)$ in $\{z, |\arg(z)| \geqslant \frac{2}{3}\pi\}$. So only formulae (43) and (46) are really necessary.

We have compared results of calculation of the Airy functions using different formulae with results obtained from the series (32)–(35) (performing computation in high-precision arithmetic `complex*32`) and thus determined their precision. In table 10 we give domains for evaluation of $\mathrm{Ai}(z)$ and $\mathrm{Bi}(z)$, which lead to a relative precision of at least 10^{-13} in the result (using `complex*16 arithmetic`).

Table 10. Ranges for evaluation of $\mathrm{Ai}(z)$, $\mathrm{Bi}(z)$ for complex z.

	Ai	Bi
$z \in A$	Series	Series
$z \in B$	$n = 20$	Series
$z \in D_1 \cup D_6$	$n = 10$	$n = 10 +$ relations
$z \in D_3 \cup D_4$	$n = 10 +$ relations	$n = 10$
$z \in D_2 \cup D_5$	$n = 10 +$ relations	$n = 10 +$ relations

Definition of the domains A, B and D_1–D_6 is given below. Let k_1 and k_2 denote the following two curves in the complex z-plane:

$$k_1 = \left\{ r\mathrm{e}^{\mathrm{i}\varphi};\ r = 3.7 + 4.5\left(\frac{1}{2} + \left| D\left(\frac{3}{2}\left(\frac{\varphi}{\pi} + 1\right)\right)\right|\right)^2; \varphi \in \langle -\pi, \pi)\right\}$$

$$k_2 = \left\{ r\mathrm{e}^{\mathrm{i}\varphi}; r = -\frac{3}{\varphi^2 - 1.5}; \varphi \in \langle -1.22, 1.22\rangle\right\}$$

where the function $D(c)$ for real c is a distance from the nearest integer number. Curve k_2 divides the interior of k_1 into two parts A and B, where A contains the origin, $z = 0$. The exterior of k_1 is divided by rays $\arg(z) = \pm\frac{\pi}{3}$ and $\arg(z) = \pm\frac{2\pi}{3}$ into six parts D_1–D_6 (anticlockwise and $10 + \mathrm{i} \in D_1$).

References

[1] Kukulin V I, Krasnopolsky V M and Horáček J 1989 *Theory of Resonances. Principles and Applications.* (Dordrecht: Kluwer)
[2] Domcke W 1991 *Phys. Rep.* **208** 97
[3] Newton R G 1982 *Scattering Theory of Waves and Particles* (Berlin: Springer)
[4] Doolen G D, Nuttall J and Stagat R W 1974 *Phys. Rev.* A **10** 1612
[5] Chu S I and Datta K K 1982 *J. Chem. Phys.* **76** 5307
[6] Reinhardt W P 1982 *Ann. Rev. Phys. Chem.* **33** 223
[7] Ho Y K 1983 *Phys. Rep.* **99** 1
[8] Christoffel K M and Bowman J M 1983 *J. Chem. Phys.* **78** 3952
[9] Mandelstam V A, Ravani T R and Taylor H S 1993 *Phys. Rev. Lett.* **70** 1932
[10] Hazi A U and Taylor H S 1970 *Phys. Rev.* A **1** 1109
[11] Truhlar D G 1974 *Chem. Phys. Lett.* **26** 377
[12] Maier C H, Cederbaum L S and Domcke W 1980 *J. Phys. B: At. Mol. Phys.* **13** L119
[13] Simons J 1981 *J. Chem. Phys.* **75** 2465
[14] McCurdy C W and McNutt J F 1983 *Chem. Phys. Lett.* **94** 306
[15] Isaacson A D and Truhlar D G 1984 *Chem. Phys. Lett.* **110** 130
[16] Macias A and Riera A 1984 *Phys. Lett.* **103A** 377
[17] Lefebvre R 1985 *J. Phys. Chem.* **89** 4201
[18] Tucker S C and Truhlar D G 1987 *J. Chem. Phys.* **86** 6251
[19] Lefebvre R 1988 *J. Phys. B: At. Mol. Opt. Phys.* **21** L709
[20] Krasnopolsky V M, Kukulin V I and Horáček J 1985 *Czech. J. Phys.* B **35** 805
[21] Čížek M and Horáček J 1996 *Czech. J. Phys.* **46** 55
[22] Siegert A F J 1939 *Phys. Rev.* **56** 750
[23] Bain R A, Bardsley J N, Junker B R and Sukumar C V 1974 *J. Phys. B: At. Mol. Phys.* **7** 2189
[24] Isaacson A D, McCurdy C W and Miller W H 1978 *Chem. Phys.* **34** 311
[25] Yaris R, Lovett R and Winkler P 1979 *Chem. Phys.* **34** 29
[26] Meyer H-D and Walter O 1982 *J. Phys. B: At. Mol. Phys.* **15** 3647
[27] Isaacson A D 1984 *Chem. Phys.* **85** 367
[28] Fernández F M 1995 *J. Phys. A: Math. Gen.* **28** 4043
[29] Connerade J-P and Lane A M 1988 *Rep. Prog. Phys.* **51** 1439
[30] Horáček J 1989 *J. Phys. A: Math. Gen.* **22** 355
[31] Humblet J 1961 *Nucl. Phys.* **26** 529
[32] Humblet J 1970 *Nucl. Phys.* A **151** 225
[33] Humblet J 1972 *Nucl. Phys.* A **187** 65
[34] Aquilera-Navarro V C, Alves N A, Zimerman A H and Ley Koo E 1986 *J. Phys. B: At. Mol. Phys.* **19** 2979
[35] Zinn-Justin J 1971 *Phys. Rep.* **10** 33
[36] Gazdy B 1976 *J. Phys. A: Math. Gen.* **9** L39
[37] Junker B R 1980 *Phys. Rev. Lett.* **44** 1487
[38] Killingbeck J 1980 *Phys. Lett.* **78A** 235
[39] Korsch H J, Laurent H and Möhlenkaupf 1981 *Mol. Phys.* **43** 1441
[40] Korsch H J, Laurent H and Möhlenkaupf 1982 *J. Phys. B: At. Mol. Phys.* **15** 1

[41] Durand Ph and Paidarová 1996 *I Comptes Rendus de l'Academie de Science (Paris)* in press
[42] Press W H, Teukolsky S A, Vetterling W T and Flannery B P 1992 *Numerical Recipes in FORTRAN, The Art of Scientific Computing* 2nd edn (Cambridge: Cambridge University Press) p 360
[43] Gradshteyn I S, Ryzhik I M 1965 *Tables of Integrals, Series and Products* (New York)
[44] Gordon R G 1968 *J. Math. Phys.* **9** 655
[45] Gordon R G 1969 *J. Chem. Phys.* **51** 14
[46] Gordon R G 1971 *Meth. Comput. Phys.* **10** 82
[47] Abramowitz M and Stegun I A 1972 *Handbook of Mathematical Functions* (New York)